Crystallographic and Thermodynamic Analysis of the Binding of *S*-Octylglutathione to the Tyr 7 to Phe Mutant of Glutathione *S*-Transferase from *Schistosoma japonicum*[†,‡]

Montserrat Andújar-Sánchez,[§] Alex W. Smith,[||] Josefa María Clemente-Jimenez,[§] Felipe Rodriguez-Vico,[§] Francisco Javier Las Heras-Vazquez,[§] Vicente Jara-Pérez,[§] and Ana Cámara-Artigas*[,§]

Departamento Química Física, Bioquímica y Química Inorgánica, Universidad de Almería, España, and Department of Chemistry and Biochemistry, Arizona State University, Tempe, Arizona 85287

Received August 6, 2004; Revised Manuscript Received October 13, 2004

ABSTRACT: Glutathione *S*-transferases are a family of multifunctional enzymes involved in the metabolism of drugs and xenobiotics. Two tyrosine residues, Tyr 7 and Tyr 111, in the active site of the enzyme play an important role in the binding and catalysis of substrate ligands. The crystal structures of *Schistosoma japonicum* glutathione *S*-transferase tyrosine 7 to phenylalanine mutant [SjGST(Y7F)] in complex with the substrate glutathione (GSH) and the competitive inhibitor *S*-octylglutathione (*S*-octyl-GSH) have been obtained. These new structural data combined with fluorescence spectroscopy and thermodynamic data, obtained by means of isothermal titration calorimetry, allow for detailed characterization of the ligand-binding process. The binding of *S*-octyl-GSH to SjGST(Y7F) is enthalpically and entropically driven at temperatures below 30 °C. The stoichiometry of the binding is one molecule of *S*-octyl-GSH per mutant dimer, whereas shorter alkyl derivatives bind with a stoichiometry of two molecules per mutant dimer. The SjGST(Y7F)·GSH structure showed no major structural differences compared to the wild-type enzyme. In contrast, the structure of SjGST(Y7F)·*S*-octyl-GSH showed asymmetric binding of *S*-octyl-GSH. This lack of symmetry is reflected in the lower symmetry space group of the SjGST(Y7F)·*S*-octyl-GSH crystals ($P6_3$) compared to that of the SjGST(Y7F)·GSH crystals ($P6_322$). Moreover, the binding of *S*-octyl-GSH to the A subunit is accompanied by conformational changes that may be responsible for the lack of binding to the B subunit.

Glutathione *S*-transferases (GSTs, EC 2.5.1.18) are a family of multifunctional dimeric enzymes involved in the detoxification of harmful physiological and xenobiotic compounds. They catalyze the nucleophilic addition of glutathione (GSH)[1] to the electrophilic center of both endo- and xenobiotic toxins. The conjugation of GSH to such molecules increases their solubility and facilitates further metabolic processing (*1*−*4*). In addition, GSTs can function as ligand-binding proteins involved in intracellular storage and transport (*5*). The precise functions of GST binding to nonsubstrate ligands remains unclear (*6*−*9*).

In recent years, GSTs from a variety of organisms have been the subject of intense research and have been classified into at least 13 different classes (*4*). Cytosolic GSTs of mammals have been particularly well-characterized and were originally classified into α, μ, π, and θ classes on the basis of a combination of criteria such as substrate−inhibitor specificity, primary and tertiary structural similarities, and immunological identity. The intraclass amino acid sequence identity ranges from 60 to 80%, while interclass homology is considerably lower (25−35%). A number of GST crystal structures have been determined in recent years, extending the structure−function knowledge of this enzyme (*3*, *10*). Despite the low sequence identity among these different classes, these proteins share a two-domain structure. The N-terminal domain I has an α/β structure, consisting of four β strands and three α helices. Domain II, a larger α domain, has five to six α helices. The active site can be further subdivided into the glutathione-binding (G site) and hydrophobic substrate-binding (H site) sites. The same or similar residues are involved in the G site of all GST classes. On the contrary, three-dimensional structures of all five GST classes [α (*11*), μ (*12*), π (*13*, *14*), θ (*15*), and σ (*16*)] show that the H site is quite different and the variability in this

[†] This work was supported in part by DGICYT Team SAF2001-2067 and BIO-2003 04274 from Dirección General Científica y Técnica, Ministerio de Ciencia y Tecnología, Spain and Plan Andaluz de Investigación Team CVI-292.

[‡] The crystallographic coordinates have been deposited in the Brookhaven Protein Data Bank under the filenames 1U87 and 1U88.

* To whom correspondence should be addressed. Telephone: 34-950015623. Fax: 34-950015008. E-mail: acamara@ual.es.

[§] Universidad de Almería.

[||] Arizona State University.

[1] Abbreviations: SjGST, *Schistosoma japonicum* glutathione *S*-transferase; SjGST(Y7F), *Schistosoma japonicum* glutathione *S*-transferase tyrosine 7 to phenylalanine mutant; GSH, glutathione; *S*-octyl-GSH, *S*-octylglutathione; *S*-hexyl-GSH, *S*-hexylglutathione; *S*-butyl-GSH, *S*-butylglutathione; *S*-propyl-GSH, *S*-propylglutathione; *S*-methyl-GSH, *S*-methylglutathione; CDNB, 1-chloro-2,4-dinitrobenzene; SEC, size-exclusion chromatography; ITC, isothermal titration calorimetry; ASA, accessible surface area; MES, 2-(*N*-morpholino)ethanesulfonic acid; ACES, *N*-(2-acetamido)-2-aminoethanesulfonic acid; TRIS, tris-(hydroxymethyl)aminomethane; PIPES, piperazine-*N*,*N*′-bis-2-ethanesulfonic acid; PDB, Protein Data Bank; rmsd, root-mean-square deviation.

10.1021/bi0483110 CCC: $30.25
Published on Web 01/05/2005

site largely accounts for the wide range of substrate specificities of GSTs. The same variability has been observed for the nonsubstrate-binding site (L site) located in the dimer interface of GSTs from *Schistosoma japonica* (*17*) and squid (*18*), near the G site of *Arabidopsis* GST (*19*), and next to the H site in human GST P1-1 isozyme (*20*).

Schistosoma japonicum GST (SjGST) is more similar in sequence and structure to the μ class than any other class of GST, although SjGST shares a number of biochemical properties with the α, μ, and π classes of GSTs (*4*). The crystal structure of SjGST has been determined for the apoenzyme (*17*) and for complexes with the physiological substrate GSH (*21*) or nonsubstrate ligands (*22*). Tyr 7 (or equivalent in other GST sequences) is one of the most conserved residues in the G site and has been postulated to play a central role in the catalytic mechanism of GSTs by stabilizing the thiolate anion of GSH and enhancing the nucleophilicity of the thiolate anion versus the protonated thiol. In the α class of GSTs, it has been proposed that this amino acid plays a role in the interaction between the G and H sites through a conformational change upon substrate binding in the G site (*23*).

Isothermal titration calorimetry (ITC) has been widely used to obtain thermodynamic information related to the binding process in biological macromolecules (*24*) and has been used as an important tool for understanding the correlation between structure and thermodynamic parameters (*25*, *26*). ITC measurements have been performed with native SjGST to characterize the binding of GSH and a number of *S*-alkyl-GSHs (*27*, *28*). Previous results have shown that the mutation of Tyr 7 to Phe results in the enzyme binding GSH with a higher affinity than the wild-type enzyme (*29*, *30*), and it has been postulated that another Tyr residue in the active site may play an important role in the binding of GSH. Moreover, this mutant shows similar fluorescence quenching upon binding of GSH, which has been attributed to a charge-transfer process between a Tyr residue and the thiol group of GSH (*31*). To date, no structure for SjGST mutants have been reported. Here, we present the structures of the SjGST tyrosine 7 to phenylalanine mutant [SjGST(Y7F)]·GSH and SjGST(Y7F)·*S*-octylglutathione (*S*-octyl-GSH) complexes as well as fluorescence and ITC studies of the binding of various *S*-alkyl-GSH inhibitors to SjGST and SjGST(Y7F). We analyze the binding of these inhibitors in light of the new structural information available, where it is shown for first time that a large GSH conjugate molecule binds in a manner that interacts with amino acids from the SjGST(Y7F) dimer interface that forms part of the L site. This binding produces conformational changes that may be responsible for the lack of binding to the second subunit.

The role that GSTs play in the binding of different ligands is an important factor related to the function of these enzymes. The overexpression of GSTs, particularly the π class of GST, has been proposed as one of the biochemical mechanisms responsible for drug resistance in cancer chemotherapy. Inhibition of overexpressed GST has been suggested as an approach to combat GST-induced drug resistance. Moreover, schistosomiasis, the disease cause by helminth worms of the genus *Schistosoma*, is a very costly and widespread parasitic disease of the developing world. A better knowledge of the binding process of GST can assist in a rational design of therapeutic drugs (*25*).

MATERIALS AND METHODS

Chemicals. All chemicals used were analytical-grade and were obtained either from Sigma Aldrich Química (Madrid, Spain) or Merck Farma y Química (Barcelona, Spain). GSH Sepharose 4B and the Superdex 200HR 10/30 column were obtained from Amersham Biosciences (Barcelona, Spain). Site-directed mutagenesis, expression, and purification were conducted as previously described (*29*).

Protein Concentration and Enzyme Assays. The concentration of both SjGST and SjGST(Y7F) was measured spectrophotometrically at 278 nm, using the extinction coefficients of 3.5×10^4 and 3.56×10^4 M^{-1} cm^{-1} for the SjGST and SjGST(Y7F) monomers, respectively (Andújar-Sánchez et al., 2003). Enzyme activity toward 1-chloro-2,4-dinitrobenzene (CDNB) was assayed at 25 °C using the Habig and Jakoby method (*32*).

Crystallization. SjGST in 0.2 M sodium citrate (pH 5.6) and 1 mM dithiothreitol (DTT) was concentrated to a final concentration of 20 mg/mL using a Microcon YM-10 (Millipore, Billerica, MA). Crystals were grown using the sitting-drop vapor-diffusion method at room temperature in 24-well plates using a modified version of the conditions previously described by McTigue et al. (*17*). Briefly, 10 μL of reservoir solution (1 mL of 0.2 M sodium citrate, 2 M ammonium sulfate, 10 mM DTT, and 10 mM threalose at pH 5.6) was mixed with 10 μL of concentrated protein solution. For the SjGST(Y7F)·*S*-octyl-GSH complex, a saturating amount of *S*-octyl-GSH (0.01 mM) was added to the protein solution. The mixture was centrifuged at 14000*g* for 5 min to remove precipitated protein and mixed with an equal volume of the reservoir solution. To avoid excessive nucleation, ethanol (2% v/v) was added to the reservoir solution. Crystals appeared after 1−3 days and grew as hexagonal rods with maximal dimensions of $0.5 \times 0.2 \times 0.2$ mm.

Data Collection, Refinement, and Model Building. Diffraction data were collected at 295 K on a Rigaku R-AXIS IV++ image-plate area detector using Cu Kα radiation from a Rigaku RU-200HB rotating-anode X-ray generator (50 kV and 100 mA). The X-ray source was equipped with an Osmic confocal mirror assembly. Images were collected as 1° rotations about the crystallographic 6-fold axis, and the data were processed with MOSFLM (*33*) and scaled with SCALA (*34*). SjGST(Y7F)·GSH complex crystals belong to the hexagonal space group $P6_322$, with unit cell parameters $a = b = 123.05$ and $c = 72.51$ Å, and contain one SjGST monomer per asymmetric unit resulting in an approximate solvent content of 59% (*35*). The SjGST(Y7F)·*S*-octyl-GSH complex crystals belong to the hexagonal space group $P6_3$, with unit cell parameters $a = b = 116.1$ and $c = 73.2$ Å, and contain two SjGST(Y7F) monomers per asymmetric unit resulting in an approximate solvent content of 55%. The structures of the SjGST(Y7F)·GSH and SjGST(Y7F)·*S*-octyl-GSH were solved by molecular replacement techniques with CNS (*36*). The coordinates for wild-type SjGST [Protein Data Bank (PDB) code 1GTA] with the water molecules removed were used as a search model. After successful identification of each orientation solution, the structures were refined using CNS package. Rigid-body refinement was performed before positional refinement using data with $F_o > 2\sigma$ in the resolution range of 30−4 Å. Cycles of positional

Table 1: Data Collection and Refinement Statistics for the SjGST(Y7F)·GSH and SjGST(Y7F)·*S*-Octyl-GSH Complexes

	SjGST(Y7F)·GSH	SjGST(Y7F)·*S*-octyl-GSH
space group	$P6_322$	$P6_3$
cell dimensions		
a (Å)	123.05	116.10
b (Å)	123.05	116.10
c (Å)	72.51	73.20
maximum resolution (Å)	3.5	3.5
number of observations	37 326	15 203
number of unique reflections	4301	5760
data completeness (%)	97.9 (97.9)	82.5 (82.5)
R_{merge}[b] (%)	17 (59)	15 (47)
$I/\sigma(I)$	3.8 (1.3)	5.7 (1.9)
protein residues	209	418
R (%)	20	22
R_{free} (%)	28	31
rmsd from ideal geometry		
bonds (Å)	0.008	0.009
angles (degrees)	1.42	1.64
mean *B* (protein) (Å^2)		
main chain	37.7	36.0
side chain	39.9	36.5
residues in favored regions of Ramachandran plot (%)[c]	100	99.5

[a] The values in parentheses are for the highest resolution bin. [b] $R_{merge} = \sum_{hkl}\sum_i|I_i - |I||$, where I_i is the intensity for the *i*th measurement of an equivalent reflection with indices *h*, *k*, and *l*. [c] From PROCHECK statistics.

and temperature-factor refinements using the resolution range 30−3.5 Å were alternated with manual building using the resulting σA-weighted ($2F_o - F_c$) and ($F_o - F_c$) electron-density maps and the program O (*37*). Electron density for the bound substrate (GSH) was visible in the G site for the SjGST(Y7F)·GSH complex. The tyrosine 7 to phenylalanine mutation was confirmed by a lack of electron density in the area where the hydroxyl group of Tyr 7 should be. The final model contains 216 of 218 amino acid residues and the substrate GSH with an *R* factor of 0.20 ($R_{free} = 0.28$). Because of the low resolution (3.5 Å), no attempt to model water molecules was made.

Because the asymmetric unit of the SjGST(Y7F)·*S*-octyl-GSH complex crystals contained two GST monomers, noncrystallographic symmetry restraints were used on all non-hydrogen atoms during the initial rounds of refinement. The inspection of the electron-density maps ($2F_o - F_c$, $F_o - F_c$, and simulated annealing omit map) showed major differences between some loops in subunit A and B; therefore, no noncrystallographic symmetry restraints were applied to the amino acids in those loops. In subunit B, the electron density is poor for amino acids 110−120 and the carboxyl terminal residues. The H-site region of subunit B is distorted and has relatively high *B* factors compared to the average *B* factor of the entire structure. Interpretable electronic density for the inhibitor *S*-octyl-GSH was found in subunit A but not in subunit B; therefore, only one molecule of *S*-octyl-GSH was modeled in subunit A. The final model contains 209 of 218 amino acid residues and the inhibitor *S*-octyl-GSH with an *R* factor of 0.22 ($R_{free} = 0.31$). The data collection and final refinement statistics for both structures are presented in Table 1. Superposition and root-mean-square deviation (rmsd) analysis of the structures were performed using the CCP4 program LSQKAB (*38*). PROCHECK (*39*) was used for stereochemical analysis of the refined structures.

Calculation of Solvent-Accessible Surface Areas. Accessible surface area (ASA) values were computed using the modeled three-dimensional structures of SjGST(Y7F) complexed with the studied inhibitors as described (*40*) using NACCESS (*41*), with a probe radius of 1.4 Å and a slice width of 0.05 Å. This program allowed us to calculate the ASA values according to the algorithm defined by Lee and Richards (*42*). The changes in the ASA upon complex formation, ΔASA, were calculated using the equation

$$\Delta ASA = ASA_{complex} - (ASA_{GST} + ASA_L)$$

where $ASA_{complex}$ is the water-accessible surface of the SjGST(Y7F)−inhibitor complex, ASA_{GST} is the water-accessible surface of the protein alone, and ASA_L is the water-accessible surface of the inhibitor. This calculation was done for the two types of surface areas, nonpolar and polar. Because the functional entity for the GSTs is the dimer and the binding site is at the interface of the dimer, the coordinates of the dimer were used for all of the calculations. The coordinates for the *S*-hexylglutathione (*S*-hexyl-GSH) complex where taken from the PDB (1M9A) where the Tyr 7 residue was truncated to Phe. To calculate the ASA for the SjGST(Y7F)·*S*-octyl-GSH complex, the coordinates from this study were used. There are no available coordinates for SjGST(Y7F)·*S*-methylglutathione (*S*-methyl-GSH); therefore, the structure for this complex was modeled from the SjGST-(Y7F)·GSH and SjGST(Y7F)·*S*-octyl-GSH complexes by deletion of the alkyl chain carbon atoms.

Size-Exclusion Chromatography−High-Performance Liquid Chromatography (SEC−HPLC). To determine the aggregation state after *S*-alkyl-GSH binding, SEC−HPLC experiments were performed with SjGST and SjGST(Y7F) in 20 mM 2-(*N*-morpholino)ethanesulfonic acid (MES), 1 mM ethylenediaminetetraacetic acid (EDTA), and 2 mM DTT at pH 6.5 in the presence of a saturating concentration of each inhibitor (0.1 mM for *S*-methyl-GSH, *S*-propylglutathione (*S*-propyl-GSH), and *S*-butylglutathione (*S*-butyl-GSH) and 0.01 mM for *S*-hexyl-GSH and *S*-octyl-GSH). Experiments were performed in a HPLC system (Breeze HPLC System, Waters, Barcelona, Spain) using a Superdex 200 HR 10/30 column. Samples of 40 μM SjGST and

SjGST(Y7F) were dialyzed for 24 h against each buffer before sample injection. Protein elution was monitored at 280 nm. Molecular-mass determination was performed using protein standards: β-amylase (200 kDa), alcohol dehydrogenase (148 kDa), ovalbumine (44 kDa), and ribonuclease A (14 kDa).

Fluorescence Emission Spectra of S-Alkyl-GSH Binding to SjGST and SjGST(Y7F). Fluorescence emission spectra were measured at 25 °C in a Perkin−Elmer LS55 spectrofluorimeter. The temperature of the cuvette holder was controlled with a temperature-controlled circulating water bath. Intrinsic fluorescence of the protein was measured by recording the emission spectra using an excitation wavelength of 280 nm, and fluorescence was monitored at 339 nm. An excitation wavelength of 295 nm was used to selectively excitate tryptophan residues. Tryptophan-specific fluorescence was monitored at 350 nm. The excitation bandwidth was 2.5 nm, and the emission bandwidth was 5 or 10 nm. The binding constant for each *S*-alkyl-GSH was determined using the measured decrease/increase in tryptophan fluorescence upon ligand binding. The observed fluorescence intensity at each dilution was corrected for the emission intensity of free enzyme. The saturation fraction of the ligand bound to the total protein was determined from the change in the ratio of ligand-bound and free-enzyme fluorescence intensity. Binding constant values (K) were determined using eq 1

$$\theta = \frac{[S\text{-alkyl-GSH}]_{free}K}{1 + [S\text{-alkyl-GSH}]_{free}K} \quad (1)$$

where θ is the saturation fraction and $[S\text{-alkyl-GSH}]_{free}$ is the free concentration of inhibitor. Data were analyzed as described previously (*23*).

Spectroscopic Determination of Tyr pK_a. The pK_a of the active-site tyrosines in SjGST were determined from the ratio 305:335 nm of fluorescence intensity emission spectra, using λ_{exc} = 280 nm. At this wavelength, both tyrosine and tyrosinate have the same absorption; therefore, the correction for screening effect is not needed (*43*). The maximum emission of tyrosine and tyrosinate residues occurs at 305 and 335 nm, respectively. Therefore, the fluorescence intensity ratio of these wavelengths represents the change in the protonation state of the tyrosine residues. Samples contained 2 μM SjGST or SjGST(Y7F) in a 50 mM buffer [phosphate, tris(hydroxymethyl)aminomethane (TRIS), and glycine] solution were measured alone or with the inhibitor at 25 °C within the appropriate range of pH values. Samples were stored in the buffer for at least 1 h prior to data acquisition. Titration data were fitted to an equation describing either a single or double ionization using Origin software.

ITC Experiments. ITC enables the determination of thermodynamic parameters, association constants, and stoichiometry of binding by direct measurement of the released or absorbed heat. ITC experiments were conducted as described in Andújar et al. (*29*). Briefly, solutions of SjGST-(Y7F) in 2 mM DTT, 1 mM EDTA, and 20 mM buffer at pH 6.5 were titrated with *S*-octyl-GSH dissolved in the same buffer. Four different buffers [*N*-(2-acetamido)-2-aminoethanesulfonic acid (ACES), MES, phosphate, and piperazine-*N*,*N*′-bis-2-ethanesulfonic acid (PIPES)] were used at pH 6.5 to measure the enthalpy of ionization of protons released or taken up by the binding process. To calculate the change in heat capacity (ΔC_p), the titration was performed at four different temperatures. Similar experiments were also conducted with *S*-methyl-GSH and *S*-hexyl-GSH, but in these cases, only three temperatures and the phosphate buffer were used. Phosphate buffer is known to have a small enthalpy of ionization (ΔH_{ioniz} = 1.22 kcal mol^{-1}) in conjunction with a small pK_a change with rising temperature (ΔpK_a/dT = −0.0028 K^{-1}). Therefore, only small corrections to the observed binding enthalpy ΔH_{obs} were required to take into account the possible protonation/deprotonation effects upon binding.

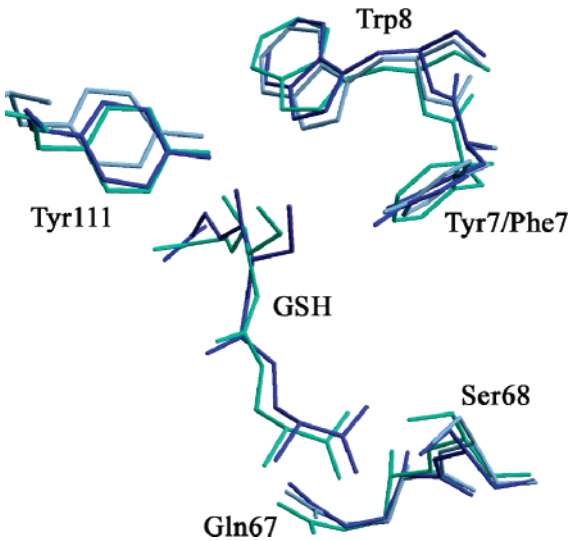

FIGURE 1: SjGST(Y7F) GSH-binding site. Superposition of the coordinates of SjGST with GSH (from PDB code 1GNE, blue) and without GSH (from PDB code 1GTA, light blue) and SjGST(Y7F) (light green). Upon binding, a displacement of Tyr 111 takes place in both the wild-type and mutant enzyme. In SjGST(Y7F), a displacement of the thiol group of GSH toward Tyr 111 increases the distance between the mutated residue (Tyr7Phe) and the substrate at the same time that a twist of ~30° at the aromatic ring of the phenylalanine takes place. [This figure was created with Pymol (*56*)].

RESULTS

SjGST(Y7F)·GSH and SjGST(Y7F)·S-Octyl-GSH Complex Structures. The overall structure of the SjGST(Y7F) complexed with the substrate GSH is essentially the same as that of the native enzyme as illustrated in Figure 1. The rmsd of the Cα positions from those of the native enzyme (PDB code 1GTA) is 0.5 Å for all 209 residues in the mutant model. However, there are some significant local changes in the G and H sites as a consequence of the Y7F mutation (Figure 1). Phe 7 is moved away from the thiol group of GSH at the same time that Tyr 111 is moved a short distance toward the GSH thiol. In wild-type SjGST, the distance between the thiol group of GSH and the hydroxyl group of Tyr 111 is 5.43 Å, whereas the distance between these two groups in SjGST(Y7F) is 4.08 Å.

The structure of the SjGST(Y7F)·*S*-octyl-GSH complex (Figure 2) was solved using a lower symmetry space group ($P6_3$). The asymmetric unit of the $P6_3$ crystal is composed of two SjGST(Y7F) molecules, related by a 2-fold noncrystallographic symmetry, that form the functional dimer. The differences observed between subunits A and B in the

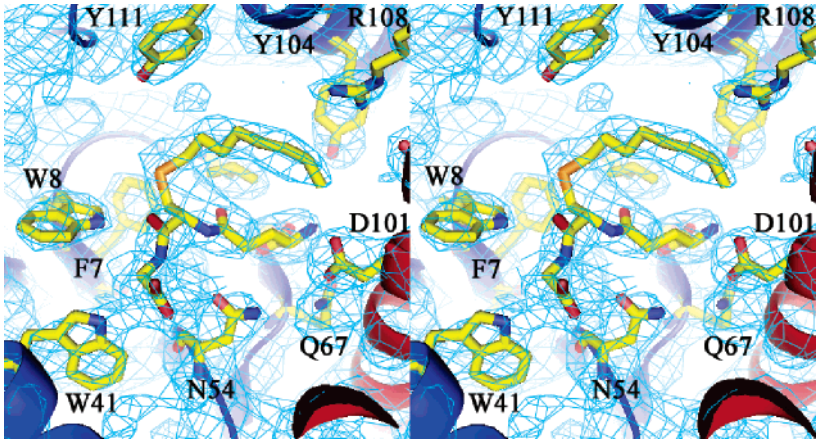

FIGURE 2: SjGST *S*-octyl-GSH-binding site. $2F_o - F_c$ electron-density map of the complex of SjGST(Y7F)·*S*-octyl-GSH, with molecule A (blue), molecule B (red), and *S*-octyl-GSH. Selected residues in contact with the inhibitor are shown. [This figure was created with Pymol (*56*)].

SjGST(Y7F)·*S*-octyl-GSH complex were not present in the native structure, where the dimer arises from the crystallographic symmetry of the $P6_322$ space group. The differences between the SjGST(Y7F)·GSH and SjGST(Y7F)·*S*-octyl-GSH structures were limited to the B subunit and include poor electron density for residues 110−120 and C-terminal residues, as well as a lack of electron density for the bound *S*-octyl-GSH.

Binding of S-Alkyl-GHSs to SjGST(Y7F): Fluorescence. The binding of *S*-alkyl-GSHs to wild-type SjGST and SjGST(Y7F) was observed by monitoring the change in intrinsic fluorescence as a function of the ligand concentration at 25 °C and pH 6.5, following the procedure outlined in the Materials and Methods. SjGST has 14 Tyr and 4 Trp residues, and fluorescence spectra results mainly from the emission of the indole ring of trytophan residues. In SjGST, two Tyr residues, Tyr 7 and Tyr 111, are in proximity to the binding site of *S*-alkyl-GSHs, whereas, in SjGST(Y7F), only one Tyr residue is present. In an effort to isolate the Tyr component of the fluorescence spectrum, the emission spectra resulting from $\lambda_{exc} = 280$ nm was compared to the emission spectra resulting from $\lambda_{exc} = 295$ nm. Experimental data from the tryptophan emission spectra were fit to eq 1 (Figure 3), and the resulting binding constants are provided in Table 2. The fluorescence-binding experiments show two different behaviors upon the binding of *S*-alkyl-GSHs. These differences were dependent on the length of the alkyl chain and excitation wavelength. When the shorter chain length inhibitors are used (methyl and propyl chains) with $\lambda_{exc} = 295$ nm, a significant quenching of fluorescence is observed, while the binding of longer chain *S*-alkyl-GSH (butyl, hexyl, and octyl) results in an enhancement of fluorescence for both the wild-type and mutant enzyme. The increased fluorescence associated with the binding of long chain *S*-alkyl-GSHs has been previously reported for the binding of *S*-hexyl-GSH to rat GSTA1-1 (*44*). The results obtained from SjGST(Y7F) using $\lambda_{exc} = 280$ nm show clear fluorescence quenching for all of the inhibitors except *S*-octyl-GSH. On the other hand, SjGST shows a different behavior at $\lambda_{exc} = 280$ nm, with only *S*-methyl-GSH causing fluorescence quenching. The Hill plot for all of the experiments yields a Hill coefficient near unity, indicating that the binding of all *S*-alkyl-GSHs to SjGST and SjGST(Y7F) is noncooperative.

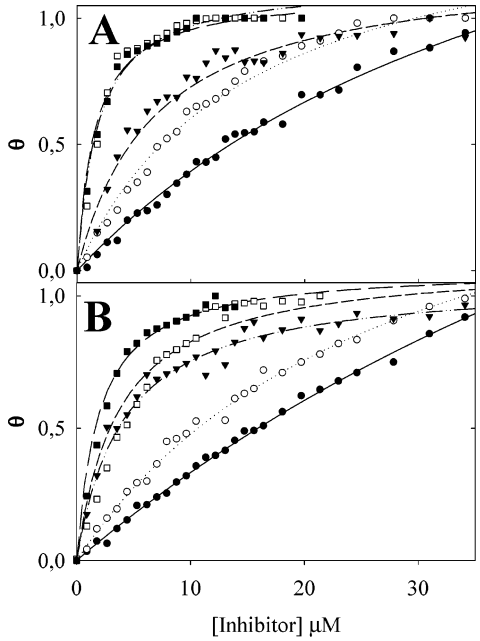

FIGURE 3: Fluorescence titration of the *S*-alkyl-GSH binding to SjGST and SjGST(Y7F). A total of 2 μM SjGST (A) or SjGST-(Y7F) (B) in 20 mM MES, 2 mM DTT, and 1 mM EDTA (pH 6.5) at 25 °C was titrated by addition of *S*-alkyl-GSH inhibitors in the same buffer: *S*-methyl-GSH (●), *S*-propyl-GSH (○), *S*-butyl-GSH (▼), *S*-hexyl-GSH (□), and *S*-octyl-GSH (■). Line plots are the fitting curves using a noncooperative model with two sites (*S*-hexyl-GSH, *S*-butyl-GSH, *S*-propyl-GSH, and *S*-methyl-GSH) or one site (*S*-octyl-GSH).

Table 2: *S*-Alkyl-GSH Binding to SjGST and SjGST(Y7F)

	SjGST K (M^{-1})	SjGST(Y7F) K (M^{-1})
S-methyl-GSH	$2.2 \pm 0.2 \times 10^4$	$4.4 \pm 0.1 \times 10^4$
S-propyl-GSH	$4.0 \pm 0.1 \times 10^4$	$4.5 \pm 0.2 \times 10^4$
S-butyl-GSH	$2.8 \pm 0.1 \times 10^5$	$2.7 \pm 0.1 \times 10^5$
S-hexyl-GSH	$6.2 \pm 0.1 \times 10^5$	$2.1 \pm 0.2 \times 10^5$
S-octyl-GSH	$5.1 \pm 0.1 \times 10^5$	$4.9 \pm 0.1 \times 10^5$

A structural feature common to nearly all GSTs is a conserved hydrogen bond between the hydroxyl group of the catalytic Tyr or Ser and the thiol group of GSH. This hydrogen bond contributes to the lowering of the pK_a of GSH from approximately 9.3 in solution to 6.4−7.4 in the active site of several GSTs (*45*). It has been proposed that Tyr 7

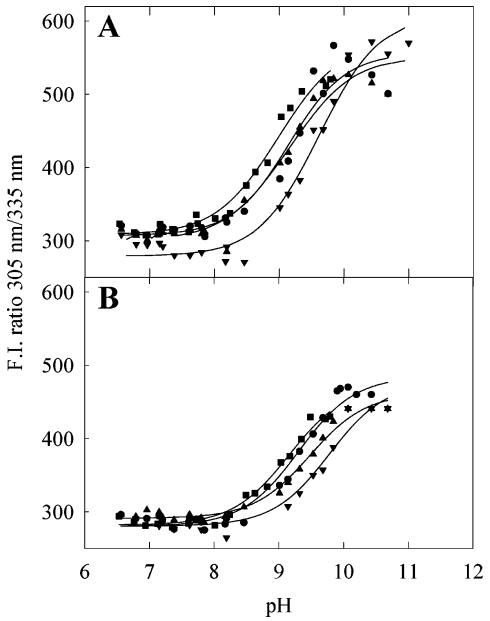

FIGURE 4: Effect of GSH and *S*-alkyl-GSH conjugates on the pK_a of the Tyr present in the active site of SjGST (A) and SjGST-(Y7F) (B). The enzyme concentration was 2 μM. Titrations were performed in the presence of none (▲) or saturating concentrations of the substrate 0.1 mM GSH (▼), 0.02 mM *S*-methyl-GSH (●), and 0.02 mM *S*-octyl-GSH (■).

Table 3: SjGST and SjGST(Y7F) Tyrosine pK_a Values

	SjGST		SjGST(Y7F)
ligand	pK_a1	pK_a2	pK_a
none	9.1 ± 0.2	9.3 ± 0.1	9.3 ± 0.1
GSH	8.7 ± 0.1	9.3 ± 0.1	9.2 ± 0.1
S-methyl-GSH	8.8 ± 0.2	9.4 ± 0.1	9.5 ± 0.1
S-octyl-GSH	9.3 ± 0.2	9.9 ± 0.1	9.8 ± 0.1

or its equivalent in other GSTs is responsible for lowering the pK_a of GSH. An additional change thought to occur upon binding of GSH is a decrease in the pK_a of Tyr 7, while the pK_a of Tyr 111 remains unchanged (*22*, *46*). To determine if the binding of *S*-alkyl-GSHs modifies the pK_a of the tyrosine residues in the GSH-binding sites of SjGST, tyrosine titration experiments were conducted in the presence of GSH and *S*-alkyl-GSHs. The amplitude of the titration curves for wild-type SjGST is almost twice that of those obtained for SjGST(Y7F) (Figure 4); therefore, titration curves for SjGST-(Y7F) were fit to a one-proton titration curve, while wild-type SjGST data were fit to a two-proton titration curve (Table 3). There is a small decrease in the pK_a of one of the two tyrosine residues upon binding of GSH to the wild-type enzyme, but no changes in the pK_a of the single tyrosine residue of the mutant enzyme were detected. The pK_a of 8.7 determined for SjGST agrees with that obtained for Tyr 9 of rat GST A1-1 (pK_a = 8.3−8.5) (*47*). A slight increase in the pK_a of one tyrosine is observed as the alkyl chain is increased in length (ΔpK_a = 0.5 from free enzyme to the enzyme·*S*-octyl-GSH complex) for both the wild-type and mutant enzyme. The same behavior has been observed in rat GST A1-1 upon addition of *S*-hexyl-GSH (*47*).

Binding of S-Alkyl-GHS to SjGST(Y7F): ITC Experiments. Independent estimates of the thermodynamic parameters governing the binding of *S*-methyl-GSH, *S*-hexyl-GSH, and *S*-octyl-GSH to SjGST(Y7F) were determined by direct calorimetric measurements performed at different temperatures, ranging from 20 to 35 °C. ITC data were analyzed using the Origin data analysis package, and data were fit using a single set of sites model. All of the parameters were allowed to float freely during fitting. A typical ITC profile for the binding of *S*-octyl-GSH to SjGST(Y7F) with the raw and integrated data for the titration in 20 mM MES, 2 mM DTT, and 1 mM EDTA (pH 6.5) at 30 °C is provided in Figure 5. These data are representative of the exothermic binding of *S*-alkyl-GSHs to SjGST(Y7F). The smooth solid line represents the best fit of the experimental data to a model of one binding site per enzyme dimer with a microscopic association constant (K) and the standard enthalpy change (ΔH_{obs}). Thermodynamic parameters of the binding of *S*-alkyl-GSHs to SjGST(Y7F) are provided in Table 4. The calorimetrically determined binding constant of *S*-alkyl-GSH to SjGST(Y7F) agrees with that obtained from fluorescence measurements. The binding of *S*-methyl-GSH and *S*-hexyl-GSH to SjGST(Y7F) is noncooperative within the temperature range analyzed and has stoichiometry of two molecules of inhibitor per SjGST(Y7F) dimer.

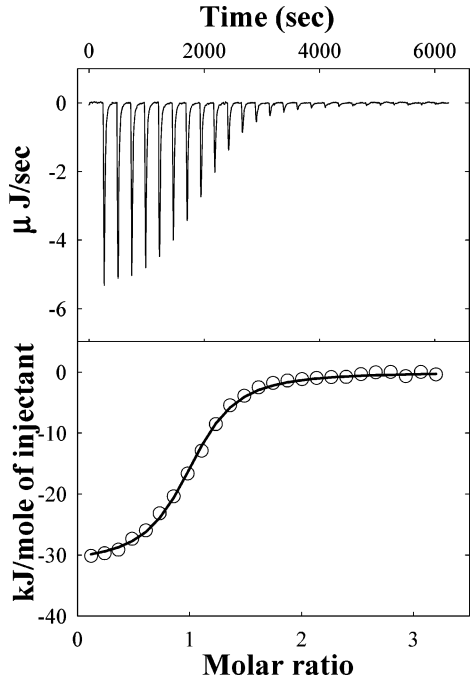

FIGURE 5: Calorimetric titration of the binding of *S*-octyl-GSH to SjGST(Y7F). Titrations were performed in 20 mM MES, 2 mM DTT, and 1 mM EDTA (pH 6.5) at 30 °C. A solution of 33.62 μM SjGST(Y7F) was titrated with 25 injections at 4-min intervals of 7 μL each of a 0.8 mM stock solution of *S*-octyl-GSH.

To study the protonation effects, calorimetric titration experiments were repeated in various buffers with different ΔH_{ioniz} (ACES, MES, phosphate, and PIPES) at pH 6.5 and a range of temperatures between 20 and 35 °C for the binding of *S*-octyl-GSH. The number of protons exchanged upon binding of *S*-octyl-GSH to SjGST(Y7F) is practically 0 (n_H = 0.1), and the measured enthalpies are equivalent to the enthalpies of binding.

A linear dependence of the binding enthalpy (ΔH_b) with the temperature was observed for the binding of the three *S*-alkyl-GSH inhibitors. The slope of this straight line was used to determine the change in heat capacity (ΔC_p) (Table 5). A strong dependence of ΔH_b and $T\Delta S$ with the temper-

Table 4: Thermodynamics Parameters of the Binding of *S*-Alkyl-GSHs to SjGST(Y7F)

	T (°C)	$\Delta H°_b$ (kJ/mol)	$\Delta S°$ (J/Kmol)	$\Delta G°$ (kJ/mol)	K (M^{-1})
S-methyl-GSH	25	-19.2 ± 0.5	23.5 ± 0.5	-26.2 ± 0.1	$3.9 \pm 0.2 \times 10^4$
	30	-26.5 ± 1.9	-3.2 ± 1.9	-25.5 ± 0.1	$2.5 \pm 0.2 \times 10^4$
	35	-32.4 ± 2.8	-25.7 ± 2.7	-24.5 ± 0.1	$1.4 \pm 0.2 \times 10^4$
S-hexyl-GSH	25	-31.3 ± 0.6	-3.8 ± 0.6	-30.1 ± 0.1	$1.9 \pm 0.2 \times 10^5$
	30	-36.9 ± 0.5	-22.2 ± 0.5	-30.1 ± 0.1	$1.5 \pm 0.2 \times 10^5$
	35	-42.4 ± 0.7	-38.0 ± 0.7	-30.7 ± 0.1	$1.6 \pm 0.2 \times 10^5$
S-octyl-GSH	20	-27.9 ± 0.7	14.6 ± 0.7	-32.2 ± 0.1	$5.4 \pm 0.3 \times 10^5$
	25	-30.4 ± 0.8	7.2 ± 0.8	-32.5 ± 0.1	$5.1 \pm 0.6 \times 10^5$
	30	-33.5 ± 0.6	-2.2 ± 0.6	-32.8 ± 0.1	$4.6 \pm 0.2 \times 10^5$
	35	-38.1 ± 0.7	-18.1 ± 0.7	-32.5 ± 0.1	$3.3 \pm 0.1 \times 10^5$

Table 5: ΔC_p of the Binding of *S*-alkyl-GSHs to SjGST(Y7F)

inhibitor	ΔC_p (kJ/Kmol)	ΔASA_{np}[a] (Å^2)	ΔASA_{pol}[a] (Å^2)	$\Delta C_{p,cal}$[a] (kJ/Kmol)
S-methyl-GSH	-1.32 ± 0.2	-644	-613	-0.54
S-hexyl-GSH	-1.14 ± 0.1	-1035	-621	-1.27
S-octyl-GSH	-0.74 ± 0.2	-707	-661	-0.61

[a] ΔASA_{np}, ΔASA_{pol}, and $\Delta C_{p,cal}$ were calculated using NACCESS as indicated in the Materials and Methods.

ature is observed, whereas $\Delta G°$ is almost insensitive to the change of temperature over the temperature range investigated for all of the inhibitors. A plot of ΔH_b versus $T\Delta S$ values for the binding of each *S*-alkyl-GSH at different temperatures shows a slope near unity. This behavior is common for protein−ligand processes and has been described in terms of enthalpy−entropy compensation (*48*). The values of binding enthalpies over the examined temperature ranges were always negative, while the entropies are positive at temperatures lower than 30 °C for *S*-methyl-GSH and *S*-octyl-GSH and negative for all of the temperatures assayed for *S*-hexyl-GSH. Therefore, the binding process is enthalpically and entropically driven for the inhibitors *S*-methyl-GSH and *S*-octyl-GSH at temperatures lower than 30 °C. The entropy of binding is a result of contributors from changes in conformational degrees of freedom (ΔS_{conf}), changes in solvation (ΔS_{sol}), and changes in translational, rotational, and vibrational degrees of freedom (ΔS_{mix}) (*49*): $\Delta S = \Delta S_{sol} + \Delta S_{conf} + \Delta S_{mix}$. Binding is expected to restrict the degrees of freedom of mobile and flexible groups in the interacting surfaces of *S*-alkyl-GSH and SjGST, but the favorable entropic changes upon inhibitor binding indicate desolvation of water molecules at the surface of the protein. ΔC_p is an approximate measure of the surface area buried in an association reaction and can be used to predict conformational rearrangements in associating protein molecules. Murphy and Freire (*50*) have suggested the following equation for ΔC_p:

$$\Delta C_p = 1.88\Delta ASA_{np} - 1.09\Delta ASA_{pol} \qquad (2)$$

Table 5 shows the comparison of the experimental determined ΔC_p values and the ΔC_p values obtained from eq 2 using the change in nonpolar and polar ASA calculated from NACCESS (*41*).

DISCUSSION

There are two outstanding features of the SjGST(Y7F)·*S*-octyl-GSH three-dimensional structure, as compared to the SjGST(Y7F)·GSH and other SjGSTs structures. The first is the lack of electron density for the inhibitor in the B subunit,

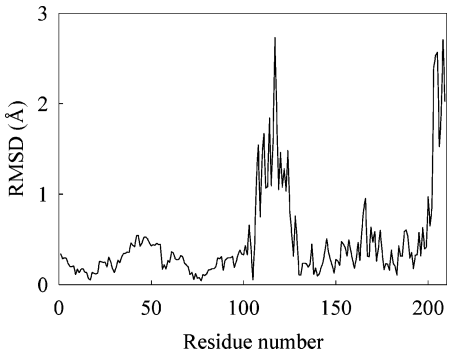

FIGURE 6: rmsd of the superposition of the main-chain atom in molecules A and B of the SjGST(Y7F)·*S*-octyl-GSH complex.

and the second is poor electron density for residues 110−120 and the C-terminal residues. A similar lack of density in the H site in one of the subunits of the GST dimer has been recently reported for the rGSTM1-1 (*51*). The lack of inhibitor density in the B subunit was proposed to arise from the different crystallographic environment of subunits A and B. In the case of rGSTM1-1, the region around the Y115F mutation, in molecule A, was stabilized by lattice interactions that constrain the area around the mutation. However, in molecule B of SjGST(Y7F)·*S*-octyl-GSH, a large number of salt bridges and hydrogen-bond contacts resulting from crystal packing are present in the complex. These contacts suggest that the differences in electron density between subunit A and B, in SjGST(Y7F)·*S*-octyl-GSH, must be caused by a different mechanism. Besides, the lack of inhibitor density in the B subunit cannot be attributed to local disorder as in the case of rGSTM1-1, where the ligand was built into both molecules of the dimer. Superposition of the SjGST(Y7F)·*S*-octyl-GSH and the SjGST·*S*-hexyl-GSH complex structures show a different orientation of the alkyl moiety (Figure 7). In SjGST·*S*-hexyl-GSH, the alkyl moiety is placed within van der Waals contacts with several residues (Tyr 7, Gly 12, Leu 13, Arg 103, Ser 107, Tyr 111, and Gln 204) (*22*). When the alkyl chain of *S*-octyl-GSH is placed in the same orientation as the hexyl chain in SjGST·*S*-hexyl-GSH, the alkyl chain of *S*-octyl-GSH is too large to fit in the same protein pocket with the two additional carbons and is placed in a new orientation with the octyl chain facing the dimer interface near the L site of SjGSTs. Fewer van der Waals contacts take place between the octyl chain and the protein residues in this orientation (only Leu 13 from chain A and Arg 108 and Asp 101 from chain B). The stoichiometry of binding apparently varies according to the size of the ligand. Because the binding process is very tight, ITC experiments allowed us to accurately determine the number of high-affinity *S*-alkyl-GSH binding sites. ITC

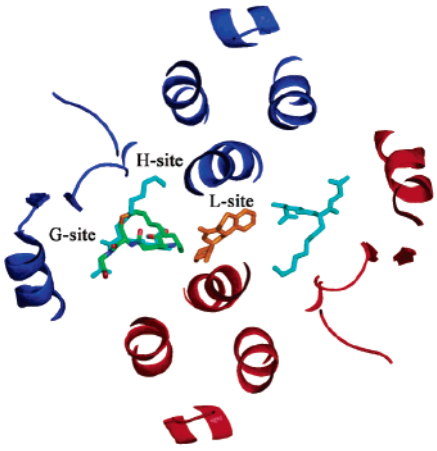

FIGURE 7: SjGST dimer. *S*-Octyl-GSH (green) binds to subunit A (blue) and interacts with the G and H sites and with the octyl chain oriented toward the L site. In SjGST, the L site has been identified by the binding of the antischistosomal drug praziquantel (orange). *S*-Hexyl-GSH (cyan) binding site in subunits A and B is shown.

results show that the stoichiometry binding of *S*-hexyl-GSH or shorter chain inhibitors is two molecules of inhibitor per SjGST(Y7F) dimer, while *S*-octyl-GSH binds with a stoichiometry of one molecule of inhibitor per SjGST(Y7F) dimer. Control experiments were conducted with the wild-type SjGST, and the resulting binding stoichiometry was the same as that of SjGST(Y7F) for the three inhibitors assayed (data not shown). As can be seen in Figure 7, *S*-octyl-GSH binds to the G and H site with the alkyl chain oriented toward the L site. Because no steric impediment is observed, the explanation for the lack of binding to the other subunit must arise from a major protein conformational change resulting from the inhibitor binding to the first subunit. The superposition of subunits A and B of the SjGST(Y7F)·*S*-octyl-GSH complex shows a major rmsd of amino acids in the entrance of the H site (aromatic residues Trp 206 and Tyr 104). These results provide evidence for a conformational change that increases the flexibility of these amino acids in the second molecule upon binding of the inhibitor to the first molecule (Figure 6).

Additional evidence for a conformational change was provided by fluorescence measurements. The fluorescence of aromatic amino acids is highly dependent on the environment where these residues are placed and provides a means to measure conformational changes that affect the environment of these residues. Our results show different behaviors for SjGST and SjGST(Y7F) when $\lambda_{exc} = 280$ nm is used, but no major differences were observed when $\lambda_{exc} = 295$ nm is used. The increase of fluorescence at $\lambda_{exc} = 295$ nm is correlated with the length of the alkyl chain. Upon binding of *S*-butyl-GSH or longer chain *S*-alkyl derivatives, the binding site becomes more hydrophobic and results in an enhancement of the tryptophan fluorescence. Using $\lambda_{exc} = 280$ nm, fluorescence quenching is observed for all of the inhibitors tested with SjGST(Y7F), except for the *S*-octyl-GSH, where an increase of fluorescence takes place. However, the wild-type enzyme only shows fluorescence quenching for the binding of GSH (*29*) and *S*-methyl-GSH. The fluorescence quenching of GSTs upon binding of GSH has been characterized as a charge transfer between the Tyr 7 (or equivalent) and the thiol group of GSH (*51*). Only two Tyr residues are within a reasonable distance of the thiol/thioether group in SjGST, but in SjGST(Y7F), only Tyr 111 can be responsible for fluorescence quenching. It has been noted that it is difficult to distinguish between tyrosinate, a strongly hydrogen-bound tyrosine, and partial-charge transfer (*52*). To investigate the protonation state of the tyrosines present in the binding site, proton tyrosine titration was conducted by means of fluorescence. These experiments show that upon binding of the substrate (GSH) a decrease in the pK_a of one of the Tyr is observed for the wild-type enzyme but no significant decrease is observed for the mutant enzyme. At the same time, the addition of long chain *S*-alkyl-GSHs results in a slight increase of the pK_a values of both enzymes. The lack of Tyr 7 in the mutant enzyme allows us to attribute the lowering of the pK_a to the Tyr 7 residue and the increasing pK_a to the Tyr 111 residue. In SjGST, a partially deprotonated Tyr 7 can be responsible for the charge transfer in the SjGST·GSH and SjGST·*S*-methyl-GSH complexes. However, in SjGST(Y7F), only Tyr 111 with a strong hydrogen bond can be responsible for fluorescence quenching. In the wild-type structure (*21*), two water molecules are within hydrogen-bond distance of the Tyr 111. In the SjGST(Y7F)·GSH model, no water molecules were modeled. Despite the absence of modeled water, the small distance between the thiol group of GSH and the hydroxyl group of Tyr 111 suggests that a water molecule bound between the thiol group of GSH and Tyr 111 would form a strongly polarized hydrogen bond. However, when a *S*-alkyl-GSH with a sufficiently large alkyl chain occupies the H site, Tyr 7 in SjGST is fully protonated and no fluorescence quenching is observed for *S*-butyl-GSH or longer chain *S*-alkyl-GSHs. SjGST is most structurally similar to the μ class of GSTs, but its H site is more similar to that of human α GST A4-4 (hGST A4-4), where the features of the H site are responsible for the specificity toward alkenals (*22*). The critical role that Tyr 212 of hGST A4-4 plays in substrate polarization has been demonstrated by means of mutagenesis analysis (*53*). The role of Tyr 212 in the α class of GSTs seems to be accomplished by Tyr 111 in SjGST.

ITC and fluorescence titration experiments show that the Y7F point mutation has little effect on the binding affinity of the *S*-alkyl-GSHs. The binding constant values obtained by means of fluorescence measurements are of the same order of magnitude as those obtained from the wild type. The binding constants are higher as the length of the alkyl chain of the inhibitors increases. The same results are obtained by means of ITC, where additional thermodynamic information is obtained. Several interactions contributed to the binding of GSH and *S*-alkyl-GSHs to SjGST(Y7F). The major difference between SjGST and SjGST(Y7F) is that the thiol group of the GSH moiety is unable to form a hydrogen bond with Tyr 7. This is supported by the correlation of the affinity constants obtained for the *S*-methyl-GSH binding to SjGST and SjGST(Y7F) as compared with the results obtained for the binding of GSH to both enzymes. In SjGST(Y7F), the binding constant of the substrate GSH ($K = 5.2 \times 10^4$ M^{-1}) is equivalent to the binding constant of the *S*-methyl-GSH ($K = 4.4 \times 10^4$ M^{-1}) and 10 times higher than that measured for the wild-type enzyme. Moreover, in SjGST, the lack of the hydrogen bond between Tyr 7 and the thiol group reduces the affinity of the inhibitor *S*-methyl-GSH ($K = 8.9 \times 10^3$ M^{-1}) (*28*). *S*-Hexyl-GSH and

S-octyl-GSH showed higher binding constants than shorter chain *S*-alkyl derivatives, but the nature of the binding interactions are slightly different for these long-chain inhibitors as shown by the thermodynamic parameters. *S*-Alkyl-GSH inhibitors show a higher hydrophobicity as the length of the alkyl chain increases. Therefore, a higher contribution of the hydrophobic effect to the binding affinity can be expected. The classic hydrophobic effect is characterized, thermodynamically, by a positive entropy change and a large negative change in ΔC_p. Meanwhile, ΔC_p values obtained experimentally agree with the characteristic of a hydrophobic effect for the three inhibitors. ΔS is negative for the binding of *S*-hexyl-GSH to SjGST(Y7F) in all of the temperature ranges studied. The origin of the negative entropy change can be attributed to a loss in side-chain configurational entropy (ΔS_{conf}) on complex formation and is associated with the restriction of a mobile side chain to a single rotamer. The movement of the alkyl chain of *S*-hexyl-GSH, upon complex formation, is more restrained than the chain of *S*-octyl-GSH upon binding to SjGST(Y7F). The hexyl chain of *S*-hexyl-GSH has more contacts with protein residues than the octyl chain of *S*-octyl-GSH. Therefore, the negative value of ΔS obtained for the SjGST(Y7F)·*S*-hexyl-GSH compared to SjGST(Y7F)·*S*-octyl-GSH can be explained by a higher configurational entropy cost in the SjGST(Y7F)·*S*-hexyl-GSH complex. Another hydrophobic effect signature, a large negative ΔC_p, is consistent with the proposal that the classical hydrophobic effect contributes to the binding free energy of the three *S*-alkyl-GSHs. The experimental values obtained by means of ITC agree well with the calculated values obtained from the ASA calculation for *S*-hexyl-GSH and *S*-octyl-GSH (Table 5). Moreover, ΔASA_{pol} is the same for the three inhibitors because it is calculated from the polar moiety in the *S*-alkyl-GSH, composed of the GSH part of the molecule. However, a higher experimental value was obtained for ΔC_p with the *S*-methyl-GSH inhibitor than calculated from the change in ASA values. This behavior has been previously reported for the binding of *S*-methyl-GSH to the wild-type SjGST and can account for a more specific interface upon binding of shorter *S*-alkyl-GSH (*28*, *54*). Moreover, the same unfavorable entropic binding with a large negative change in ΔC_p has been reported in a study of several alkyl derivatives of the pheromone 2-*sec*-butyl-4,5-dihydrothiazole to the mouse major urinary protein I (*55*), where the shorter alkyl derivatives show more negative experimental ΔC_p than the longer ones.

S-Hexyl-GSH and other shorter *S*-alkyl derivatives bind simultaneously to the G and H sites, but the longer hydrophobic alkyl chain of *S*-octyl-GSH is oriented toward the L site and is in contact with the residues of the dimer interface (Asp 101 and Arg 108 from chain B). Binding to the nonsubstrate L site has been described previously to have a stoichiometry of one molecule of ligand per dimer (*17*, *56*). This is the first time that structural evidence of a bound large *S*-alkyl-GSH conjugate interacting with amino acids in the L site located near the dimer interface has been obtained. No evidence of steric conflicts between the inhibitor molecules bound to either subunit has been found. A conformational change increasing the flexibility of amino acids near the entrance of the H site of the unbound subunit is the most likely mechanism by which the binding of *S*-octyl-GSH is inhibited in this subunit. This information opens new avenues for the design of novel drugs to fight schistosomiasis and drug resistance in cancer chemotherapy.

ACKNOWLEDGMENT

We thank Dr. James P. Allen (Arizona State University, Tempe, AZ) for assistance in performing the X-ray experiments.

REFERENCES

1. Mannervik, B., and Danielson, U. H. (1988) Glutathione transferases: Structure and catalytic activity, *Crit. Rev. Biochem. 23*, 283−337.
2. Armstrong, R. N. (1997) Structure, catalytic mechanism, and evolution of the glutathione transferases, *Chem. Res. Toxicol. 10*, 2−18.
3. Dirr, H. W., Reinemer, P., and Huber, R. (1994) X-ray crystal structures of cytosolic glutathione *S*-transferases. Implications for protein architecture, substrate recognition, and catalytic function, *Eur. J. Biochem. 220*, 645−661.
4. Sheehan, D., Meade, G., Foley, V. M., and Dowd, C. A. (2001) Structure, function, and evolution of glutathione transferases: Implications for classification of non-mammalian members of an ancient enzyme superfamily, *Biochem. J. 360*, 1−16.
5. Listowsky, I., Abramovitz, M., Homma, H., and Niitsu, Y. (1988) Intracellular binding and transport of hormones and xenobiotics by glutathione *S*-transferase, *Drug Metab. Rev. 19*, 305−318.
6. Le Trong, I., Stenkamp, R. E., Ibarra, C., Atkins, W. M., and Adman, E. T. (2002) 1.3 Å resolution structure of human glutathione *S*-transferase with *S*-hexyl glutathione bound reveals possible extended ligandin binding site, *Proteins 48*, 618−627.
7. Sayed, Y., Hornby, J. A., Lopez, M., and Dirr, H. (2002) Thermodynamics of the ligandin function of human class α glutathione transferase A1-1: Energetics of organic anion ligand binding, *Biochem. J. 363*, 341−346.
8. Sayed, Y., Wallace, L. A., and Dirr, H. W. (2000) The hydrophobic lock-and-key intersubunit motif of glutathione transferase A1-1: Implications for catalysis, ligandin function, and stability, *FEBS Lett. 465*, 169−172.
9. Sluis-Cremer, N., Wallace, L., Burke, J., Stevens, J., and Dirr, H. (1998) Aflatoxin B1 and sulphobromophthalein binding to the dimeric human glutathione *S*-transferase A1-1: A fluorescence spectroscopic analysis, *Eur. J. Biochem. 257*, 434−442.
10. Wilce, M. C. J., and Parker, M. W. (1994) Structure and function of glutathione *S*-transferases, *Biochim. Biophys. Acta 1205*, 1−18.
11. Sinning, I., Kleywegt, G. J., Cowan, S. W., Reinemer, P., Dirr, H. W., Huber, R., Gilliland, G. L., Armstrong, R. N., Ji, X., Board, P. G., Olin, B., Mannervick, B., and Jones, A. (1993) Structure determination and refinement of human α class glutathione transferase A1-1, and a comparison with the μ and π class enzymes, *J. Mol. Biol. 232*, 192−212.
12. Ji, X., Zhang, P., Armstrong, R. N., and Gilliland, G. L. (1992) The three-dimensional structure of a glutathione *S*-transferase from the μ gene class. Structural analysis of the binary complex of isoenzyme 3-3 and glutathione at 2.2 Å resolution, *Biochemistry 31*, 10169−10184.
13. Reinemer, P., Dirr, H. W., Ladenstein, R., Schaffer, J., Gallay, O., and Huber, R. (1991). The three-dimensional structure of class π glutathione *S*-transferase in complex with glutathione sulfonate at 2.3 Å resolution, *EMBO J. 10*, 1997−2005.
14. Reinemer, P., Dirr, H. W., Ladenstein, R., Huber, R., Lo Bello, M., Federici, G., and Parker, M. W. (1992) Three-dimensional structure of class π glutathione *S*-transferase from human placenta in complex with *S*-hexylglutathione at 2.8 Å resolution, *J. Mol. Biol. 227*, 214−226.
15. Wilce, M. C. J., Board, P. G., Feil, S. C., and Parker, M. W. (1995) Crystal structure of a θ-class glutathione transferase, *EMBO J. 14*, 2133-2143.
16. Ji, X., von Rosenvinge, E. C., Johnson, W. W., Tomarev, S. I., Piatigorsky, J., Armstrong, R. N., and Gilliland, G. L. (1995) Three-dimensional structure, catalytic properties, and evolution of a σ class glutathione transferase from squid, a progenitor of the lens *S*-crystallins of cephalopods, *Biochemistry 34*, 5317−5328.
17. McTigue, M. A., Williams, D. R., and Tainer, J. A. (1995) Crystal structures of a schistosomal drug and vaccine target: Glutathione

S-transferase from *Schistosoma japonica* and its complex with the leading antischistosomal drug praziquantel, *J. Mol. Biol. 246*, 21−27.
18. Ji, X., von Rosenvinge, E. C., Johnson, W. W., Armstrong, R. N., and Gilliland, G. L. (1996) Location of a potential transport binding site in a σ class glutathione transferase by X-ray crystallography, *Proc. Natl. Acad. Sci. U.S.A. 93*, 8208−8213.
19. Reinemer, P., Prade, L., Hof, P., Neuefeind, T., Huber, R., Zettl, R., Palme, K., Schell, J., Koelln, I., Bartunik, H. D., and Bieseler, B. (1996) Three-dimensional structure of glutathione *S*-transferase from *Arabidopsis thaliana* at 2.2 Å resolution: Structural characterization of herbicide-conjugating plant glutathione *S*-transferases and a novel active site architecture, *J. Mol. Biol. 255*, 289−309.
20. Oakley, A. J., Lo Bello, M., Nuccetelli, M., Mazzetti, A. P., and Parker, M. W. (1999) The ligand in (non-substrate) binding site of human π class glutathione transferase is located in the electrophile binding site (H-site), *J. Mol. Biol. 291*, 913−926.
21. Lim, K., Ho, J. X., Keeling, K., Gilliland, G. L., Ji, X., Ruker, F., and Carter, D. C. (1994) Three-dimensional structure of *Schistosoma japonicum* glutathione *S*-transferase fused with a six-amino acid conserved neutralizing epitope of gp41 from HIV, *Protein Sci. 3*, 2233−2244.
22. Cardoso, R. M., Daniels, D. S., Bruns, C. M., and Tainer, J. A. (2003) Characterization of the electrophile binding site and substrate binding mode of the 26-kDa glutathione *S*-transferase from *Schistosoma japonicum*, *Proteins 51*, 137−146.
23. Nieslanik, B. S., and Atkins, W. M. (2000) The catalytic Tyr-9 of glutathione *S*-transferase A1-1 controls the dynamics of the C terminus, *J. Biol. Chem. 275*, 17447−17451.
24. Leavitt, S., and Freire, E. (2001) Direct measurement of protein binding energetics by isothermal titration calorimetry, *Curr. Opin. Struct. Biol. 11*, 560−566.
25. Ladbury, J. E. (2001) Isothermal titration calorimetry: Application to structure based drug design, *Thermochim. Acta 380*, 209−215.
26. Velazquez-Campoy, A., Kiso, Y., and Freire, E. (2001) The binding energetics of first- and second-generation HIV-1 protease inhibitors: Implications for drug design, *Arch. Biochem. Biophys. 390*, 169−175.
27. Ortiz-Salmeron, E., Yassin, Z., Clemente-Jimenez, M. J., Las Heras-Vazquez, F. J., Rodriguez-Vico, F., Baron, C., and Garcia-Fuentes, L. (2001) Thermodynamic analysis of the binding of glutathione to glutathione *S*-transferase over a range of temperatures, *Eur. J. Biochem. 268*, 4307−4314.
28. Ortiz-Salmeron, E., Yassin, Z., Clemente-Jimenez, M. J., Las Heras-Vazquez, F. J., Rodriguez-Vico, F., Baron, C., and Garcia-Fuentes, L. (2001) A calorimetric study of the binding of *S*-alkylglutathiones to glutathione *S*-transferase, *Biochim. Biophys. Acta 1548*, 106−113.
29. Andújar-Sánchez, M., Clemente-Jimenez, J. M., Las Heras-Vazquez, F. J., Rodriguez-Vico, F., Cámara-Artigas, A., and Jara-Pérez, V. (2003) Thermodynamics of glutathione binding to the tyrosine 7 to phenylalanine mutant of glutathione *S*-transferase from *Schistosoma japonicum*, *Int. J. Biol. Macromol. 32*, 77−82.
30. Andújar-Sánchez, M., Clemente-Jimenez, J. M., Rodriguez-Vico, F., Las Heras-Vazquez, F. J., Jara-Pérez, V., and Cámara-Artigas, A. (2004) A monomer form of the glutathione *S*-transferase Y7F mutant from *Schistosoma japonicum* at acidic pH, *Biochem. Biophys. Res. Commun. 314*, 6−10.
31. Dietze, E. C., Ibarra, C., Dabrowski, M. J., Bird, A., and Atkins, W. M. (1996) Rational modulation of the catalytic activity of A1-1 glutathione *S*-transferase: Evidence for incorporation of an on-face ($\pi\cdots$HO−Ar) hydrogen bond at tyrosine-9, *Biochemistry 35*, 11938−11944.
32. Habig, W. H., and Jakoby W. B. (1981) Assays for determination of glutathione-*S*-transferase, *Methods Enzymol. 77*, 398−405.
33. Leslie, A. G. W. (1990) Recent changes to the MOSFLM package for processing film and image plate data. CCP4 and ESF-EACMB Newsletter on Protein Crystallography, Daresbury, Warrington, U.K.
34. Kabsch, W. (1988) Evaluation of single-crystal X-ray diffraction data from a position sensitive detector, *J. Appl. Crystallogr. 21*, 916−924.
35. Matthews, B. W. (1968) Solvent content of protein crystals, *J. Mol. Biol. 33*, 491−497.
36. Brünger, A. T., Adams, P. D., Clore, G. M., DeLano, W. L., Gros, P., Grosse-Kunstleve, R. W., Jiang, J. S., Kuszewski, J., Nilges, M., Pannu, N. S., Read, R. J., Rice, L. M., Simonson, T., and Warren, G. L. (1998) Crystallography and NMR system: A new software suite for macromolecular structure determination, *Acta Crystallogr., Sect. D 54*, 905−921.
37. Jones, T. A., Zou, J.-Y., Cowan, S. W., and Kjeldgard, M. (1991) Improved methods for building protein models in electron density maps and the location of errors in these models, *Acta Crystallogr., Sect. A 47*, 110−119.
38. Kabsch, W. (1976) Solution for best rotation to relate 2 sets of vectors, *Acta Crystallogr., Sect. A 32*, 922−923.
39. Laskowski, R. A., McArthur, M. W., Moss, D. S., and Thorton, J. M. (1993) PROCHECK: A program to check the stereochemical quality of protein structures, *J. Appl. Crystallogr. 26*, 283−291.
40. Makhatadze, G. I., and Privalov, P. L. (1995) Energetics of protein structure, *Adv. Protein Chem. 47*, 307−425.
41. Hubbard, S. J., and Thornton, J. M. (1993) *NACCESS*, Department of Biochemistry and Molecular Biology, University College London, London, U.K.
42. Lee B., and Richards F. M. (1971) The interpretation of protein structures: Estimation of static accessibility, *J. Mol. Biol. 55*, 379−400.
43. Permyakov, E. A. (1993) *Luminescent Spectroscopy of Proteins*, CRC Press, Boca Raton, FL.
44. Wang, R. W., Bird, A. W., Newton, D. J., Lu, A. Y., and Atkins, W. M. (1993) Fluorescence characterization of Trp 21 in rat glutathione *S*-transferase 1-1: Microconformational changes induced by *S*-hexyl glutathione, *Protein Sci. 2*, 2085−2094.
45. Nilsson, L. O., Gustafsson, A., and Mannervik, B. (2000) Redesign of substrate-selectivity determining modules of glutathione transferase A1-1 installs high catalytic efficiency with toxic alkenal products of lipid peroxidation, *Proc. Natl. Acad. Sci. U.S.A. 97*, 9408−9412.
46. Hubatsch, I., and Mannervik, B. (2001) A highly acidic tyrosine 9 and a normally titrating tyrosine 212 contribute to the catalytic mechanism of human glutathione transferase A4-4, *Biochem. Biophys. Res. Commun. 280*, 878−882.
47. Atkins, W. M., Wang, R. W., Bird, A. W., Newton, D. J., and Lu, A. Y. (1993) The catalytic mechanism of glutathione *S*-transferase (GST). Spectroscopic determination of the pK_a of Tyr-9 in rat α 1-1 GST, *J. Biol. Chem. 268*, 19188−19191.
48. Brummell, D. A., Sharma, V. P., Anand, N. N., Bilous, D., Dubuc, G., Michniewicz, J., Roger MacKenzie, C., Sadowska, J., Sigurskjold, B. W., Sinnot, B., Young, N. M., Bundle, D. R., and Narang, S. A. (1993) Probing the combining site of an anti-carbohydrate antibody by saturation-mutagenesis: Role of the heavy-chain CDR3 residues, *Biochemistry 32*, 1180−1187.
49. Murphy, K. P. (1999) Predicting binding energetics from structure: Looking beyond ΔG, *Med. Res. Rev. 19*, 333−339.
50. Murphy, K. P., and Freire, E. (1992) Thermodynamics of structural stability and cooperative folding behavior in proteins, *Adv. Protein Chem. 43*, 313−361.
51. Codreanu, S. G., Ladner, J. E., Xiao, G., Stourman, N. V., Hachey, D. L., Gilliland, G. L., and Armstrong, R. N. (2002) Local protein dynamics and catalysis: Detection of segmental motion associated with rate-limiting product release by a glutathione transferase, *Biochemistry 41*, 15161−15172.
52. Dietze, E. C., Wang, R. W., Lu, A. Y., and Atkins, W. M. (1996) Ligand effects on the fluorescence properties of tyrosine-9 in α 1-1 glutathione *S*-transferase, *Biochemistry 35*, 6745−6753.
53. Bruns, C. M., Hubatschm, I., Ridderstrom, M., Mannervik, B., Tainer, J. A. (1999) Human glutathione transferase A4-4 crystal structures and mutagenesis reveal the basis of high catalytic efficiency with toxiclipid peroxidation products, *J. Mol. Biol. 288*, 427−439.
54. Ladbury, J. E., Wright, J. G., Sturtevant, J. M., and Sigler, P. B. (1994) A thermodynamic study of the trp repressor−operator interaction, *J. Mol. Biol. 238*, 669−681.
55. Sharrow, S. D., Novotny, M. V., and Stone, M. J. (2003) Thermodynamic analysis of binding between mouse major urinary protein-I and the pheromone 2-*sec*-butyl-4,5-dihydrothiazole, *Biochemistry 42*, 6302−6309.
56. DeLano, W. L. *The PyMOL Molecular Graphics System*, DeLano Scientific LLC, San Carlos, CA, http://www.pymol.org.

BI0483110